THE JOURNAL OF PHYSICAL CHEMISTRY C

Article

pubs.acs.org/JPCC

Direct Spectroscopic Evidence for Constituent Heteroatoms Enhancing Charge Recombination at a TiO_2–Ruthenium Dye Interface

Ke Hu,[†] Holly A. Severin,[‡] Bryan D. Koivisto,[‡] Kiyoshi C. D. Robson,[‡] Eduardo Schott,[∥] Ramiro Arratia-Perez,*[,§] Gerald J. Meyer,*[,†] and Curtis P. Berlinguette*[,‡,⊥]

[†]Departments of Chemistry and Materials Science and Engineering, Johns Hopkins University, 3400 North Charles Street, Baltimore, Maryland 21218, United States

[‡]Department of Chemistry, University of Calgary, 2500 University Drive NW, Calgary, Alberta, Canada T2N 1N4

[§]Departamento de Ciencias Químicas, Relativistic Molecular Physics Group, Universidad Andres Bello, Republica 275, Santiago, Chile

[⊥]Departments of Chemistry and Chemical & Biological Engineering, The University of British Columbia, 2036 Main Mall, Vancouver, British Columbia, Canada V6T1Z1

[∥]Laboratorio de Bionanotecnología, Universidad Bernardo O'Higgins, General Gana 1780, Santiago, Chile

Supporting Information

ABSTRACT: A series of three bis(tridentate) cycloruthenated sensitizers with furyl, thiophene, or selenophene units attached to the cyclometalated ligand were designed to examine how chalcogen atoms effect interfacial electron transfer events that occur following the absorption of visible light by the sensitizers when attached to mesoporous titania thin films immersed in CH_3CN electrolytes. Spectroelectrochemistry established that the $Ru^{III/II}$ reduction potentials were confined to the 0.954–0.965 V vs NHE range for the series and that the density of TiO_2 acceptor states were sensitizer-independent. Pulsed light excitation into the metal-to-ligand charge transfer band of the sensitized thin films resulted in rapid excited state injection, $k_{inj} > 10^8\ s^{-1}$. Charge recombination ($Ru^{III}/TiO_2(e^-) \rightarrow Ru^{II}/TiO_2$) rate constants were insensitive to the identity of the cyclometalated compound, yet the open circuit photovoltages were markedly lower for the compound containing selenophene. These lower photovoltages appear to be a manifestation of a 4-fold-larger, second-order rate constant measured for the reaction between triiodide and $TiO_2(e^-)$ in the case that the selenophene comprises the donor fragment of the dye. Adduct formation between oxidized iodide(s) and the selenophene moiety of the sensitizer is implicated.

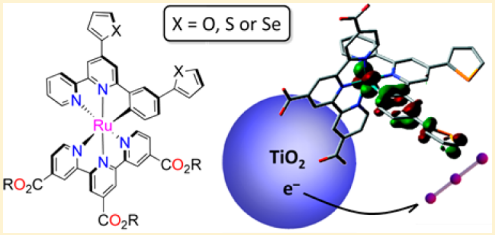

INTRODUCTION

Interfacial processes at the titania photoanode in a dye-sensitized solar cell (DSSC) are sensitive to a myriad of factors.[1−3] The electron promoted by light from a dye into titania is ideally collected at the transparent conducting glass substrate and returned to an oxidized dye by a redox mediator that is in intimate contact with the counter electrode.[4] These injected electrons, however, can also be intercepted by the small concentration of photo-oxidized dyes on the surface[5−7] or by the oxidized form of the redox shuttle (e.g., I_2, I_3^-).[8,9] A lower open-circuit voltage (V_{oc}) is often attributed to the latter recombination event, which can be suppressed by aliphatic substituents tethered to the dye molecules that serve to inhibit redox-active species from reaching the semiconductor surface.[10,11] The measured photovoltages are also intimately related to the regeneration of the photooxidized dyes by the electrolyte.[5]

Resolving the recombination and regeneration processes that manifest as lower photovoltages in operational devices is complicated by the dynamic nature of the cell. Regeneration of dyes by I^-, for example, most likely involves the formation of an adduct with the dye.[12−14] A consequence of this adduct formation is that specific chemical components of the dye may alter interfacial electron transfer kinetics and, in turn, device efficiency. We recently elaborated on such a feature for a pair of metal-free triarylamine-based donor–π-bridge–acceptor molecules that differed only in the identity of two heteroatoms, sulfur and oxygen, comprising the donor unit of the respective dyes (Figure 1).[5] Although this study demonstrated that sulfur atoms can have a measurable effect on photovoltages, particularly at the power point or open circuit conditions where competitive recombination pathways play a more prominent role, a seemingly contrarian observation was made earlier by O'Regan and co-workers[8] when they showed that sulfur atoms in a common ruthenium-based dye scaffold

Special Issue: Michael Grätzel Festschrift

Received: January 24, 2014
Revised: April 11, 2014
Published: May 1, 2014

   dx.doi.org/10.1021/jp500879p | J. Phys. Chem. C 2014, 118, 17079–17089

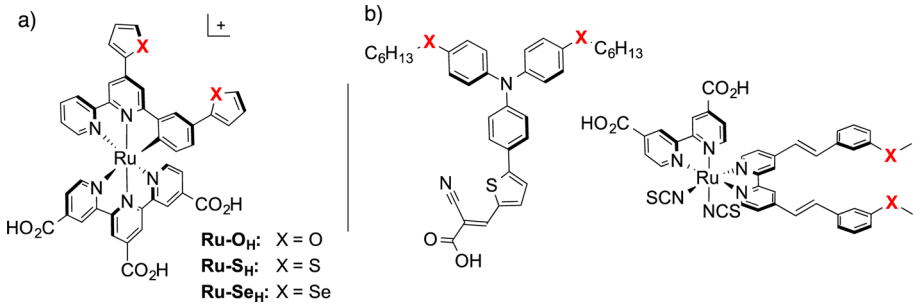

Figure 1. (a) Series of ruthenium chromophores Ru–X (X = O, S, Se) used in this study. (b) Previously documented dyes used to probe interfacial electron transfer (X = O, S).[5,8]

enhanced recombination with I_3^- or I_2. We conjecture that the relative positions of the heteroatoms account for these apparent disparities; namely, the organic dyes presented in Figure 1 involve a heteroatom change within the donor unit that is positioned away from the surface and spatially optimized for reaction with the electrolyte, whereas the ruthenium scaffold positions the sulfur atom closer to the titania surface and away from the anionic NCS^- ligands that are a more likely site for regeneration.[8]

We therefore set out to reconcile these experimental differences by examining how heteroatoms, carefully positioned within the donor units of otherwise structurally related ruthenium-based dyes, impact both regeneration and recombination. The unique series of bis(tridentate) cycloruthenated dyes used for this study contain terminal furyl, thiophene, and selenophene substituents (Figure 1) that offer the opportunity to examine how interfacial electron transfer kinetics are affected for a series of metal-based dyes with uniform optical and electrochemical properties. It was found that changing the chalcogen within the five-membered rings of these terminal substituents did not impact the regeneration step, as we had anticipated at the outset of the study. Notwithstanding, transient spectroscopic methods indicate that the more polarizable selenophene unit increases the rate of recombination with I_3^-, thereby compromising the measured photovoltages. We attribute these observations to the close proximity of the chalcogen atoms within the flanking five-membered rings to the surface.

EXPERIMENTAL

Preparation of Compounds. All reagents were purchased from Aldrich and used without further purification, except for $RuCl_3 \cdot 3H_2O$ (Pressure Chemical Company) and trimethyl-4,4′,4″-tricarboxylate-2,2′:6′,2″-terpyridine (**L4**; Helios Chemical Company, Switzerland). Purification by column chromatography was carried out using silica (Silicycle: Ultrapure Flash Silica). Analytical thin-layer chromatography (TLC) was performed on aluminum-backed sheets precoated with silica 60 F254 adsorbent (0.25 mm thick; Merck, Germany) and visualized under UV light. Routine ^{1}H and ^{13}C NMR spectra were recorded at 400 and 100 MHz, respectively, on a Bruker AV 400 instrument at ambient temperatures. Chemical shifts (δ) are reported in parts per million (ppm) from low- to high-field and referenced to residual nondeuterated solvent. Standard abbreviations indicating multiplicity are used as follows: s = singlet; d = doublet; t = triplet ; m = multiplet. All proton assignments correspond to the generic molecular schemes that are provided (Figure 2). Organic precursors selenophene-2-carbaldehyde,[15] 1-(2-(3-bromophenyl)-2-oxoethyl)pyridinium iodide,[16] (*E*)-1-(pyridin-2-yl)-3-(thiophen-2-yl)prop-2-en-1-one (**P2**),[17] 2-(furan-2-yl)-4,4,5,5-tetramethyl-1,3,2-dioxaborolane (**P7**),[18] and 4,4,5,5-tetramethyl-2-(thiophen-2-yl)-1,3,2-dioxaborolane (**P8**)[19] were prepared as previously reported.

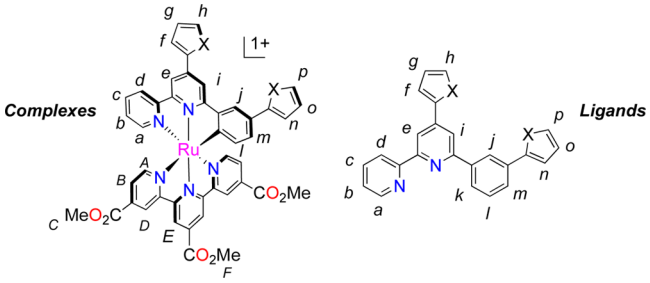

Figure 2. Labeling scheme for ^{1}H NMR signal assignments.

*(E)-3-(Furan-2-yl)-1-(pyridin-2-yl)prop-2-en-1-one (**P1**).*[17] A methanol/water (9:1; 60 mL) solution containing acetylpyridine (4.5 mL, 40 mmol), furan-2-carbaldehyde (3.3 mL, 40 mmol), and potassium hydroxide (2.14 g, 38.2 mmol) was stirred at room temperature overnight, and then the solvent was removed in vacuo. The oil residue was dissolved in DCM and washed with water/brine (1:1; 2 × 200 mL). The organic fractions were dried with $MgSO_4$, filtered, and dried in vacuo to yield a brown oil. Purification by column chromatography [SiO_2: DCM/EtOAc, 9:1; R_f = 0.86] yielded 2.6 g (33%) of the product as a yellow oil that solidified upon standing. ^{1}H NMR (400 MHz, $CDCl_3$): δ = 8.71 (ddd, 1H, ^3J = 4.7 Hz, ^4J = 1.6 Hz, ^5J = 0.9 Hz, H_a), 8.15–8.09 (m, 2H, H_d, H_β), 7.83 (dt, 1H, ^3J = 7.7 Hz, ^4J = 1.7 Hz, H_c), 7.67 (d, 1H, ^3J = 15.8 Hz, H_e), 7.51 (d, 1H, ^3J = 1.5 Hz, H_h), 7.44 (ddd, 1H, ^3J = 7.6 Hz, ^4J = 4.7 Hz, ^5J = 1.2 Hz, H_b), 6.74 (d, 1H, ^3J = 3.4 Hz, H_f), 6.48 (dd, 1H, ^3J = 3.4 Hz, ^4J = 1.8 Hz, H_g). ^{13}C NMR (100 MHz, $CDCl_3$): δ = 189.3, 154.2, 152.1, 148.9, 145.1, 136.9, 130.6, 126.8, 122.8, 118.8, 116.2, 112.6. HRMS (EI): m/z = 199.0630 [$(M)^+$] (calcd for $C_{12}H_9NO_2^+$: m/z = 199.0633).

*(E)-1-(Pyridin-2-yl)-3-(selenophen-2-yl)prop-2-en-1-one (**P3**).* A methanol/water (9:1; 60 mL) solution containing acetylpyridine (2.2 mL, 19.7 mmol), selenophene-2-carbaldehyde[15] (3.12 g, 19.7 mmol), and potassium hydroxide (1.05 g, 29.7 mmol) was stirred at room temperature overnight. Vacuum filtration yielded 1.43 g (27.8%) of the product as a bright yellow powder. ^{1}H NMR (400 MHz, $CDCl_3$): δ = 8.71 (ddd, 1H, ^3J = 4.7 Hz, ^4J = 1.7 Hz, ^5J = 0.9 Hz, H_a), 8.14 (ddd, 1H, ^3J = 7.9 Hz, ^4J = 1.0 Hz, ^5J = 1.0 Hz, H_d), 8.08 (d, 1H, ^3J = 5.6 Hz, H_h), 8.05 (d, 1H, ^3J = 15.5 Hz, H_β), 7.93 (d, 1H, ^3J = 15.5 Hz, H_e), 7.83 (dt, 1H, ^3J = 7.7 Hz, ^4J = 1.7 Hz, H_c), 7.55 (d, 1H, ^3J = 3.7 Hz, H_f), 7.45 (ddd, 1H, ^3J = 7.6 Hz, ^4J = 4.7 Hz,

dx.doi.org/10.1021/jp500879p | J. Phys. Chem. C 2014, 118, 17079–17089

^5J = 1.2 Hz, H_b), 7.27 (dd, 1H, ^3J = 5.5 Hz, ^4J = 3.8 Hz, H_g). ^{13}C NMR (100 MHz, $CDCl_3$): δ = 189.2, 154.3, 149.0, 147.1, 139.6, 137.2, 135.8, 134.6, 130.9, 127.0, 123.0, 121.2. HRMS (EI): m/z = 262.9860 [$(M)^+$] (calcd for $C_{12}H_9NO^{80}Se^+$: m/z = 262.9849).

*6-(3-Bromophenyl)-4-(furan-2-yl)-2,2′-bipyridine (**P4**).* A mixture of (*E*)-3-(furan-2-yl)-1-(pyridin-2-yl)prop-2-en-1-one (**P1**) (1.74 g, 8.79 mmol), ammonium acetate (17.8 g, 228 mmol), and 1-(2-(3-bromophenyl)-2-oxoethyl)pyridinium iodide (3.55 g, 8.79 mmol) and formamide (30 mL) was slowly brought to 120 °C under a dinitrogen atmosphere with stirring. The reaction was left at 120 °C overnight and then cooled to room temperature. The precipitate was isolated by vacuum filtration and washed with EtOH. The solid was solubilized in DCM, dried with $MgSO_4$, filtered, and concentrated before being purified by column chromatography (SiO_2: DCM/EtOAC, 9:1; R_f = 0.83) to yield the product as a dark orangey-brown oil (1.87 g, 56.4%). ^{1}H NMR (400 MHz, $CDCl_3$): δ = 8.70 (d, 1H, ^3J = 5.5 Hz, H_a), 8.60 (d, 1H, ^3J = 7.9 Hz, H_d), 8.58 (d, 1H, ^4J = 1.4 Hz, H_e), 8.33 (t, 1H, ^4J = 1.8 Hz, H_j), 8.06 (d, 1H, ^3J = 8.9 Hz, H_k), 7.95 (d, 1H, ^4J = 1.4 Hz, H_i), 7.84 (td, 1H, ^3J = 7.7 Hz, ^4J = 1.8 Hz, H_c), 7.56−7.53 (m, 2H, H_h, H_m), 7.53 (t, 1H, ^3J = 7.9 Hz, H_l), 7.32 (ddd, 1H, ^3J = 7.4 Hz, ^3J = 4.8 Hz, ^4J = 1.1 Hz, H_b), 7.04 (d, 1H, ^3J = 3.4 Hz, H_f), 6.54 (dd, 1H, ^3J = 1.8 Hz, ^3J = 3.4 Hz, H_g). ^{13}C NMR (100 MHz, $CDCl_3$): δ = 156.5, 156.1, 155.6, 151.9, 149.3, 143.9, 141.5, 139.6, 137.1, 132.2, 130.4, 130.3, 125.7, 124.2, 123.2, 121.6, 114.6, 114.3, 112.4, 109.4. HRMS (EI): m/z = 376.0193 [$(M)^+$] (calcd for $C_{20}H_{13}N_2OBr^+$: m/z = 376.0211).

*6-(3-Bromophenyl)-4-(thiophen-2-yl)-2,2′-bipyridine (**P5**).* A mixture of (*E*)-1-(pyridin-2-yl)-3-(thiophen-2-yl)prop-2-en-1-one (**P2**) (2.00 g, 9.29 mmol), 1-(2-(3-bromophenyl)-2-oxoethyl)pyridinium iodide (3.75 g, 9.29 mmol), and formamide (25 mL) was stirred and slowly heated to 120 °C under a N_2 atmosphere and left under these conditions overnight. The solution was cooled to room temperature, and the solvent removed in vacuo. The remaining solids were triturated with EtOH and air-dried. The dark solid was solubilized in DCM and dried with $MgSO_4$, and the solvents were removed by rotovap. The product was purified by column chromatography (SiO_2: DCM/EtOAc, 9:1; R_f = 0.95) to yield an oil that solidified upon standing; 1.67 g (45.7%). ^{1}H NMR (400 MHz, $CDCl_3$): δ 8.70 (dd, 1H, ^3J = 4.7 Hz, ^4J = 0.8 Hz, H_a), 8.61 (m, 2H, H_e, H_d), 8.33 (t, 1H, ^4J = 1.8 Hz, H_j), 8.06 (d, 1H, ^3J = 7.8 Hz, H_k), 7.87 (d, 1H, ^4J = 1.6 Hz, H_i), 7.85 (t, 1H, ^3J = 7.8 Hz, ^4J = 1.8 Hz, H_c), 7.69 (dd, 1H, ^3J = 3.7 Hz, ^4J = 1.0 Hz, H_h), 7.56 (dq, 1H, ^3J = 7.9 Hz, ^4J = 0.9 Hz, H_m), 7.43 (dd, 1H, ^3J = 5.1 Hz, ^4J = 0.9 Hz, H_f), 7.37 (t, 1H, ^3J = 7.9 Hz, H_l), 7.33 (dd, 1H, ^3J = 4.8 Hz, ^4J = 1.1 Hz, H_b), 7.16 (dd, 1H, ^3J = 5.0 Hz, ^3J = 3.7 Hz, H_g). ^{13}C NMR (100 MHz, $CDCl_3$): δ 156.8, 156.0, 155.9, 149.3, 143.7, 141.8, 141.5, 131.2, 132.3, 130.5, 130.4, 128.6, 127.4, 125.9, 125.8, 124.3, 123.3, 121.7, 116.9, 116.4. HRMS (EI): m/z = 393.9945 [$(M)^+$] (calcd for $C_{20}H_{13}N_2SBr$: m/z = 393.9962).

*6-(3-Bromophenyl)-4-(selenophen-2-yl)-2,2′-bipyridine (**P6**).* A stirring mixture of (*E*)-1-(pyridin-2-yl)-3-(selenophen-2-yl)prop-2-en-1-one (**P3**) (1.20 g, 4.58 mmol), 1-(2-(3-bromophenyl)-2-oxoethyl)pyridinium iodide (1.85 g, 4.58 mmol), ammonium acetate (9.20 g, 119 mmol), and formamide (25 mL) was brought to 120 °C under a N_2 atmosphere and left overnight. The dark brown reaction mixture was allowed to cool to room temperature. The resulting solid was removed by vacuum filtration, and purified by column chromatography to yield 1.28 g (63.5%) of the product as a tan solid after drying in vacuo. ^{1}H NMR (400 MHz, $CDCl_3$): δ = 8.69 (ddd, 1H, ^3J = 4.8 Hz, ^4J = 1.8 Hz, ^5J = 0.9 Hz, H_a), 8.56 (ddd, 1H, ^3J = 8.0 Hz, ^4J = 1.0 Hz, ^5J = 1.0 Hz, H_d), 8.52 (d, 1H, ^4J = 1.6 Hz, H_e), 8.30 (t, 1H, ^3J = 1.8 Hz, H_j), 8.08 (dd, 1H, ^3J = 5.5 Hz, ^4J = 1.0 Hz, H_h), 8.01 (ddd, 1H, ^3J = 7.8 Hz, ^4J = 1.6 Hz, ^5J = 1.1 Hz, H_k), 7.86−7.77 (m, 2H, H_c, H_f), 7.75 (d, 1H, ^4J = 3.7 Hz, H_i), 7.54 (ddd, 1H, ^3J = 7.9 Hz, ^4J = 2.0 Hz, ^5J = 1.0 Hz, H_m), 7.38−7.28 (m, 3H, H_g, H_l, H_b). ^{13}C NMR (100 MHz, $CDCl_3$): δ = 156.5, 155.8, 155.6, 149.2, 147.9, 145.3, 141.3, 137.0, 132.8, 132.1, 131.0, 130.3, 130.2, 128.1, 125.6, 124.1, 123.2, 121.6, 117.2, 116.7. HRMS (EI): m/z = 439.9407 [$(M)^+$] (calcd for $C_{20}H_{13}N_2SeBr^+$: m/z = 439.9427).

*4,4,5,5-Tetramethyl-2-(selenophen-2-yl)-1,3,2-dioxaborolane (**P9**).* *n*-BuLi (1.6 M in hexanes, 26.2 mL, 42.0 mmol) was added dropwise to a solution of selenophene (5.00 g, 38.2 mmol) in THF (120 mL) at −78 °C. The solution was stirred for 30 min at room temperature. After cooling to −78 °C, 2-isopropoxy-4,4′,5,5′-tetrametyldioxoborolane (11.7 g, 62.9 mmol) was added, and the reaction mixture was stirred for 20 min at room temperature. The reaction was quenched with MeOH (5 mL), and the product was extracted with Et_2O. The ether layer was washed with brine (2 × 100 mL), dried with $MgSO_4$, and filtered, and the solvent was removed by rotary evaporation. The oil residue was purified by column chromatography (SiO_2: hexanes/EtOAc (9:1); R_f = 0.49) to give the product as a light yellow oil that solidified upon standing (3.54 g, 36.1%) . ^{1}H NMR (400 MHz, $CDCl_3$): δ = 8.33 (d, 1H, ^3J = 5.1 Hz, H_n), 7.95 (d, 1H, ^3J = 3.4 Hz, H_p), 7.43 (dd, 1H, ^3J = 5.1 Hz, ^3J = 3.7 Hz, H_o), 1.32 (s, 12H, CH_3). ^{13}C NMR (100 MHz, $CDCl_3$): δ = 139.6, 137.8, 131.0, 84.0, 82.8, 24.8, HRMS (EI): m/z = 258.0327 [$(M)^+$] (calcd for $C_{10}H_{15}BO_2Se^+$: m/z = 258.0330).

*4-(Furan-2-yl)-6-(3-(furan-2-yl)phenyl)-2,2′-bipyridine (**L1H**).* 2-(Furan-2-yl)-4,4,5,5-tetramethyl-1,3,2-dioxaborolane (**P7**) (1.09 g, 5.61 mmol) and 6-(3-bromophenyl)-4-(furan-2-yl)-2,2′-bipyridine (**P4**) (933 mg, 2.47 mmol) were solubilized in THF/H_2O (9:1, 125 mL) and sparged with N_2 for 10 min. K_2CO_3 (3.44 g, 24.7 mmol) and $Pd(PPh_3)_4$ (405 mg, 0.35 mmol) were then added, and the reaction was allowed to reflux for 14 h under N_2. The reaction mixture was cooled to room temperature and washed with brine. The organic layer was dried with $MgSO_4$ and then the solvent was removed in vacuo. The residue was purified by column chromatography (SiO_2: gradient elution DCM/hexanes 8:2 to DCM to DCM/EtOAc 9:1; R_f = 0.13 in 8:2 DCM/hexanes) to yield the product as a yellow oil that solidified upon standing; 715 mg (79.3%). ^{1}H NMR (400 MHz, $CDCl_3$): δ = 8.71 (d, 1H, ^3J = 4.7 Hz, H_a), 8.65 (d, 1H, ^3J = 7.9 Hz, H_d), 8.62 (s, 1H, H_e), 8.46 (s, 1H, H_j), 8.07 (d, 1H, ^3J = 7.8 Hz, H_k), 8.04 (s, 1H, H_i), 7.84 (td, 1H, ^3J = 7.7 Hz, ^3J = 1.4 Hz, H_c), 7.74 (d, 1H, ^3J = 7.8 Hz, H_m), 7.57 (s, 1H, H_h), 7.53−7.48 (m, 2H, H_g, H_l), 7.32 (dd, 1H, ^3J = 7.4 Hz, ^3J = 5.5 Hz, H_b), 7.05 (d, 1H, ^3J = 3.4 Hz, H_f), 6.78 (d, 1H, ^3J = 3.3 Hz, H_n), 6.55 (dd, 1H, ^3J = 3.2 Hz, ^3J = 1.7 Hz, H_g), 6.50 (dd, 1H, ^3J = 3.0 Hz, ^3J = 1.8 Hz, H_o). ^{13}C (100 MHz, $CDCl_3$): δ = 157.1, 156.4, 156.3, 154.1, 152.1, 149.2, 143.8, 142.4, 140.0, 139.5, 137.1, 131.5, 129.3, 126.3, 124.7, 124.1, 122.6, 121.6, 114.7, 114.0, 112.3, 111.9, 109.2, 105.6. HRMS (EI): m/z = 364.1207 [$(M)^+$] (calcd for $C_{24}H_{16}N_2O_2^+$: m/z = 364.1212).

*4-(Thiophen-2-yl)-6-(3-(thiophen-2-yl)phenyl)-2,2′-bipyridine (**3**).* 4,4,5,5-Tetramethyl-2-(thiophen-2-yl)-1,3,2-dioxabor-

dx.doi.org/10.1021/jp500879p | J. Phys. Chem. C 2014, 118, 17079−17089

olane (**P8**) (915 mg, 4.35 mmol) and 6-(3-bromophenyl)-4-(thiophen-2-yl)-2,2′-bipyridine (**P2**) (842 mg, 2.14 mmol) were solubilized in a THF/H_2O (9:1, 125 mL) mixture and sparged with N_2 for 10 min. K_2CO_3 (2.98 g, 21.4 mmol) and $Pd(PPh_3)_4$ (352 mg, 0.30 mmol) were then added, and the reaction was allowed to reflux for 14 h under N_2. The reaction mixture was cooled to room temperature and washed with brine. The product was extracted into ether, and the organic layer was dried with $MgSO_4$. Solvents were removed in vacuo, and the oil residue was purified by column chromatography (SiO_2: gradient elution DCM/hexanes 8:2 to DCM to DCM/EtOAc 9:1; R_f = 0.26 in 8:2 DCM/hexanes) to yield the product as a yellow-brown oil that was further purified by trituration with absolute EtOH to yield 688 mg (81.0%) of a tan solid. ^{1}H NMR (400 MHz, $CDCl_3$): δ = 8.72 (dd, 1H, ^3J = 4.8 Hz, ^4J = 0.9 Hz, H_a), 8.66 (d, 1H, ^3J = 7.1 Hz, H_d), 8.63 (d, 1H, ^4J = 1.6 Hz, H_e), 8.40 (t, 1H, ^4J = 1.7 Hz, H_j), 8.05 (ddd, 1H, ^3J = 7.8 Hz, ^4J = 1.6 Hz, ^4J = 1.2 Hz, H_k), 7.95 (d, 1H, ^4J = 1.6 Hz, H_i), 7.85 (td, 1H, ^3J = 7.6 Hz, ^4J = 2.0 Hz, H_c), 7.70 (dd, 1H, ^3J = 3.7 Hz, ^4J = 1.1 Hz, H_h), 7.68 (dd, 1H, ^4J = 1.8 Hz, ^4J = 1.1 Hz, H_m), 7.52 (t, 1H, ^3J = 7.8 Hz, H_l), 7.45−7.42 (m, 2H, H_p, H_f), 7.35 (dd, 1H, ^3J = 4.4 Hz, ^4J = 1.2 Hz, H_b), 7.32 (dd, 1H, ^3J = 4.9 Hz, ^4J = 1.2 Hz, H_n), 7.16 (dd, 1H, ^3J = 5.0 Hz, ^3J = 3.7 Hz, H_g), 7.12 (dd, 1H, ^3J = 5.1 Hz, ^3J = 3.6 Hz, H_o). ^{13}C NMR (100 MHz, $CDCl_3$): δ = 157.1, 156.7, 156.2, 149.2, 144.5, 143.5, 141.9, 140.1, 137.1, 135.1, 129.5, 128.5, 128.3, 127.2, 126.9, 126.4, 125.8, 125.2, 124.9, 124.1, 123.7, 121.7, 117.0, 116.1. HRMS (EI): m/z = 396.0746 [$(M)^+$] (calcd for $C_{24}H_{16}N_2S_2^+$: m/z = 396.0755).

*4-(Selenophen-2-yl)-6-(3-(selenophen-2-yl)phenyl)-2,2′-bipyridine (**L3H**).* 6-(3-Bromophenyl)-4-(selenophen-2-yl)-2,2′-bipyridine (**P3**) (642 mg, 1.46 mmol) and 4,4,5,5-tetramethyl-2-(selenophen-2-yl)-1,3,2-dioxaborolane (**P9**) (756 mg, 2.94 mmol) were solubilized in THF/water (9:1, 125 mL) and sparged with N_2 for 10 min. K_2CO_3 (2.02 g, 14.6 mmol) and $Pd(PPh_3)_4$ (236 mg, 0.204 mmol) were then added, and the reaction was allowed to reflux under nitrogen for 14 h. The reaction mixture was then cooled to room temperature and washed with brine. The product was extracted with Et_2O. The organic layer was dried with $MgSO_4$ and filtered, and then the solvent was removed in vacuo. Purification by column chromatography [SiO_2: DCM/EtOAc (9:1); R_f = 0.34] yielded 516 mg (72.1%) of the product as an orange solid. ^{1}H NMR (400 MHz, $CDCl_3$): δ = 8.72 (ddd, 1H, ^3J = 4.8 Hz, ^4J = 1.7 Hz, ^5J = 0.9 Hz, H_a), 8.64 (d, 1H, ^3J = 8.0 Hz, H_d), 8.58 (d, 1H, ^4J = 1.5 Hz, H_e), 8.36 (t, 1H, ^3J = 1.7 Hz, H_j), 8.10 (d, 1H, ^3J = 5.6 Hz, H_h), 8.04 (d, 1H, ^3J = 7.8 Hz, H_k), 7.98 (d, 1H, ^3J = 5.5 Hz, H_p), 7.90−7.81 (m, 3H, H_c, H_f, H_i), 7.63 (d, 1H, ^4J = 7.7 Hz, H_m), 7.59 (d, 1H, ^3J = 3.7 Hz, H_n), 7.50 (t, 1H, ^3J = 7.7 Hz, H_l), 7.39 (dd, 1H, ^3J = 5.5 Hz, ^4J = 3.9 Hz, H_g), 7.36 (dd, 1H, ^3J = 5.4 Hz, ^4J = 3.8 Hz, ^5J = 1.0 Hz, H_o), 7.33 (ddd, 1H, ^3J = 7.4 Hz, ^4J = 4.8 Hz, ^5J = 1.0 Hz, H_b). ^{13}C NMR (100 MHz, $CDCl_3$): δ = 157.0, 156.6, 156.1, 150.9, 149.2, 148.2, 145.3, 140.1, 137.1, 137.0, 132.7, 131.0, 130.8, 130.5, 129.4, 128.1, 127.4, 126.4, 125.8, 125.3, 124.1, 121.6, 117.5, 116.6. HRMS (EI): m/z = 491.9639 [$(M)^+$] (calcd for $C_{24}H_{16}N_2{}^{80}Se_2^+$: m/z = 491.9644).

General Preparation of Methyl Ester Complexes (Ru−X_{Me}). To a MeOH/H_2O/THF solution (5:1:1, v/v/v, 210 mL) containing 0.40 mmol of the ligand (e.g., **L1H**—**L3H**) was added 0.40 mmol of Ru(**L4**)Cl_3 and *N*-ethylmorpholine (0.5 mL). Following a 16 h reflux, $AgNO_3$ (1.20 mmol) was added to the reaction mixture, and then the mixture was allowed to reflux for an additional 1.5 h. The mixture was then cooled and preabsorbed on silica, and the solvent was removed in vacuo. The product was purified by chromatographic techniques (details specified below). The desired fraction was collected and isolated to yield a dark red fine solid.

[Ru(L1)(L4)]NO_3 (Ru−O_{Me}). Chromatographic conditions. SiO_2: CH_2Cl_2/MeOH 9:1; R_f = 0.50. Yield = 213 mg (0.23 mmol, 57.2%). ^{1}H NMR (400 MHz, $CDCl_3$): δ = 9.14 (s, 2H, H_E), 9.08 (s, 1H, H_d), 8.96−8.88 (m, 2H, H_D, H_e), 8.47 (s, 1H, H_j), 8.07 (s, 1H, H_i), 7.96 (t, 1H, ^3J = 6.8 Hz, H_c), 7.77−7.62 (m, 6H, H_A, H_B, H_a, H_h), 7.33 (s, 1H, H_f), 7.17 (d, 1H, ^3J = 3.1 Hz, H_p), 7.03 (d, 1H, ^3J = 5.7 Hz, H_n), 6.77−6.70 (m, 2H, H_b, H_m), 6.40 (d, 1H, ^3J = 1.0 Hz, H_g), 6.34 (d, 1H, ^3J = 0.9 Hz, H_o), 5.37 (d, 1H, ^3J = 7.5 Hz, H_l), 4.18 (s, 3H, H_F), 3.92 (s, 6H, H_C). HRMS (ESI): m/z = 866.1310 [$(M)^+$] (calcd for $C_{45}H_{31}N_5O_8Ru$: m/z = 866.1321). Anal. Calcd for $C_{45}H_{32}N_6O_{11}Ru{\cdot}3H_2O$: C, 54.71; H, 3.88; N, 8.51. Found: C, 54.53; H, 3.82; N, 8.49.

[Ru(L2)(L4)]NO_3 (Ru−S_{Me}). Chromatographic conditions. SiO_2: CH_2Cl_2/MeOH 9:1; R_f = 0.36. Yield = 277 mg (0.29 mmol, 72.0%). ^{1}H NMR (400 MHz, $CDCl_3$): δ = 9.15 (s, 2H, H_E), 9.06−9.03 (m, 2H, H_d, H_e), 8.92 (d, 2H, ^4J = 1.0 Hz, H_D), 8.29 (d, 1H, ^4J = 1.2 Hz, H_i), 8.23 (dd, 1H, ^3J = 3.5 Hz, ^4J = 0.6 Hz, H_a), 7.96−7.92 (m, 2H, H_c, H_j), 7.71 (d, 2H, ^3J = 5.8 Hz, H_A), 7.65 (dd, 2H, ^3J = 5.9 Hz, ^4J = 1.6 Hz, H_B), 7.55 (d, 1H, ^3J = 5.0 Hz, H_h), 7.32 (dd, 1H, ^3J = 5.0 Hz, ^3J = 3.8 Hz, H_f), 7.22 (d, 1H, ^3J = 4.7 Hz, H_p), 7.13 (dd, 1H, ^3J = 5.0 Hz, ^4J = 0.9 Hz, H_n), 7.08 (dd, 1H, ^3J = 3.6 Hz, ^4J = 0.9 Hz, H_b), 7.06 (d, 1H, ^3J = 6.4 Hz, H_m), 6.95 (dd, 1H, ^3J = 5.0 Hz, ^3J = 3.7 Hz, H_g), 6.70 (dd, 1H, ^3J = 7.9 Hz, ^3J = 1.9 Hz, H_o), 5.39 (d, 1H, ^3J = 7.8 Hz, H_l), 4.20 (s, 3H, H_F), 3.94 (s, 6H, H_C). HRMS (ESI): m/z = 898.0849 [$(M)^+$] (calcd for $C_{45}H_{32}N_5O_6RuS_2^+$: m/z = 898.0865). Anal. Calcd for $C_{45}H_{32}N_6O_9RuS_2{\cdot}2H_2O$: C, 53.94; H, 3.62; N, 8.39. Found: C, 54.24; H, 3.67; N, 8.09.

[Ru(L3)(L4)]NO_3 (Ru−Se_{Me}). Chromatographic conditions. SiO_2: CH_2Cl_2/MeOH 9:1; R_f = 0.32. Yield = 327 mg (0.31 mmol, 77.4%). ^{1}H NMR (400 MHz, $CDCl_3$): δ = 9.15 (s, 2H, H_E), 9.05 (d, 1H, ^3J = 8.2 Hz, H_d), 8.98 (d, 1H, ^4J = 1.4 Hz, H_e), 8.92 (d, 2H, ^4J = 1.0 Hz, H_D), 8.37 (dd, 1H, ^3J = 3.8 Hz, ^4J = 0.9 Hz, H_a), 8.23 (dd, 1H, ^3J = 5.5 Hz, ^4J = 0.9 Hz, H_h), 8.20 (d, 1H, ^4J = 1.4 Hz, H_i), 7.95 (td, 1H, ^3J = 7.9 Hz, ^4J = 1.5 Hz, H_c), 7.87 (d, 1H, ^4J = 1.9 Hz, H_j), 7.78 (dd, 1H, ^3J = 5.5 Hz, ^4J = 1.0 Hz, H_p), 7.71 (d, 2H, ^3J = 5.9 Hz, H_A), 7.50 (dd, 2H, ^3J = 5.9 Hz, ^4J = 1.7 Hz, H_B), 7.55 (dd, 1H, ^3J = 5.6 Hz, ^4J = 3.9 Hz, H_f), 7.90−7.80 (m, 3H, H_g, H_m, H_n), 7.07 (ddd, 1H, ^3J = 7.5 Hz, ^4J = 5.5 Hz, ^5J = 1.0 Hz, H_b), 6.65 (dd, 1H, ^3J = 7.8 Hz, ^4J = 1.9 Hz, H_o), 5.38 (d, 1H, ^3J = 7.9 Hz, H_l), 4.22 (s, 3H, H_F), 3.96 (s, 6H, H_C). HRMS (ESI): m/z = 997.9756 [$(M)^+$] (calcd for $C_{45}H_{32}N_5Ru^{80}Se_2^+$: m/z = 997.9734). Anal. Calcd for $C_{45}H_{32}N_6O_9RuSe_2{\cdot}H_2O$: C, 50.15; H, 3.18; N, 7.80. Found: C, 49.99; H, 3.57; N, 7.51.

General Preparation of Carboxylic Acid Complexes (Ru−X_H). A solution containing 0.13 mmol of ester metal complexes (Ru−X_{Me}) in DMF/H_2O/NEt_3 (3:1:1, v/v/v, 25 mL) was refluxed for 4 h. The solution was then cooled, and the solvent was removed in vacuo. The product was triturated with DCM and collected via vacuum filtration to yield a dark red fine solid.

[Ru(L1)(L5)]NO_3 (Ru−O_H). Yield = 105 mg (0.13 mmol, 98.6%). ^{1}H NMR (400 MHz, DMSO-d_6): δ = 9.44 (s, 2H, H_E), 9.19 (s, 2H, H_D), 9.04 (s, 1H, H_e), 8.97 (d, 1H, ^3J = 8.3 Hz, H_d), 8.83 (d, 1H, ^4J = 0.6 Hz, H_j), 8.13 (d, 1H, ^3J = 1.5 Hz, H_h), 8.02 (t, 1H, ^3J = 7.9 Hz, H_c), 7.84 (d, 1H, ^3J = 3.3 Hz, H_f), 7.72

dx.doi.org/10.1021/jp500879p | J. Phys. Chem. C 2014, 118, 17079−17089

(d, 2H, ^3J = 5.9 Hz, H_A), 7.61−7.58 (m, 3H, H_B, H_p), 7.48 (d, 1H, ^3J = 4.9 Hz, H_a), 7.16 (dd, 1H, ^3J = 5.5 Hz, ^3J = 1.9 Hz, H_b), 6.95 (dd, 1H, ^3J = 3.5 Hz, ^3J = 1.8 Hz, H_g), 6.80 (dd, 1H, ^3J = 7.8 Hz, ^4J = 1.7 Hz, H_m), 6.76 (d, 1H, ^3J = 3.3 Hz, H_n), 6.49 (dd, 1H, ^3J = 3.4 Hz, ^3J = 1.8 Hz, H_o), 5.54 (d, 1H, ^3J = 7.9 Hz, H_l). HRMS (ESI): m/z = 824.0838 [$(M)^+$] (calcd for $C_{42}H_{26}N_5O_8Ru$: m/z = 824.0838). Anal. Calcd for $C_{42}H_{26}N_6O_{11}Ru{\cdot}4H_2O$: C, 52.34; H, 3.56; N, 8.72. Found: C, 52.15; H, 3.65; N, 8.57.

[Ru(L2)(L5)]NO_3 (Ru−S_H). Yield = 109 mg (0.13 mmol, 97.8%). ^{1}H NMR (400 MHz, DMSO-d_6): δ = 9.43 (s, 2H, H_E), 9.18 (s, 2H, H_D), 9.03 (d, 1H, ^3J = 8.3 Hz, H_d), 8.99 (s, 1H, H_e), 8.84 (s, 1H, H_i), 8.41 (d, 1H, ^3J = 2.8 Hz, H_h), 8.37 (d, 1H, ^4J = 1.5 Hz, H_j), 8.01 (dt, 1H, ^3J = 8.6 Hz, ^3J = 1.2 Hz, H_c), 7.94 (d, 1H, ^3J = 5.1 Hz, H_f), 7.70 (d, 2H, ^3J = 5.8 Hz, H_A), 7.58 (dd, 2H, ^3J = 5.8 Hz, ^4J = 1.2 Hz, H_B), 7.49 (dd, 1H, ^3J = 5.6 Hz, ^4J = 0.7 Hz, H_a), 7.44 (dd, 1H, ^3J = 4.8 Hz, ^3J = 3.7 Hz, H_g), 7.39 (d, 1H, ^3J = 3.4 Hz, H_p), 7.34 (d, 1H, ^3J = 4.9 Hz, H_n), 7.15 (dd, 1H, ^3J = 6.8 Hz, ^3J = 5.4 Hz, H_b), 7.02 (dd, 1H, ^3J = 4.9 Hz, ^3J = 3.7 Hz, H_o), 6.67 (d, 1H, ^3J = 7.4 Hz, H_m), 5.50 (d, 1H, ^3J = 7.8 Hz, H_l). HRMS (ESI): m/z = 856.0392 [$(M)^+$] (calcd for $C_{42}H_{26}N_5O_6RuS_2^+$: m/z = 856.0392). Anal. Calcd for $C_{42}H_{26}N_6O_9RuS_2{\cdot}4H_2O$: C, 50.65; H, 3.44; N, 8.44. Found: C, 50.55; H, 3.21; N, 8.42.

[Ru(L3)(L5)]NO_3 (Ru−Se_H). Yield = 122 mg (0.13 mmol, 98.9%). ^{1}H NMR (400 MHz, DMSO-d_6): δ = 9.47 (s, 2H, H_E), 9.23 (s, 2H, H_D), 9.07 (d, 1H, ^3J = 8.1 Hz, H_d), 8.95 (s, 1H, H_e), 8.81(s, 1H, H_i), 8.58 (d, 1H, ^3J = 3.6 Hz, H_f), 8.55 (d, 1H, ^3J = 5.6 Hz, H_h), 8.35 (d, 1H, ^4J = 1.5 Hz, H_j), 8.01 (t, 1H, ^3J = 7.7 Hz, H_c), 7.94 (d, 1H, ^3J = 5.6 Hz, Hz, H_p), 7.71 (d, 2H, ^3J = 5.9 Hz, H_A), 7.64 (dd, 1H, ^3J = 5.4 Hz, ^4J = 4.0 Hz, H_g), 7.60 (dd, 2H, ^3J = 5.8 Hz, ^4J = 1.4 Hz, H_B), 7.52 (d, 1H, ^3J = 3.6 Hz, H_n), 7.49 (d, 1H, ^3J = 5.2 Hz, H_a), 7.23 (dd, 1H, ^3J = 5.3 Hz, ^4J = 3.9 Hz, H_o), 7.15 (t, 1H, ^3J = 6.5 Hz, H_b), 6.61 (d, 1H, ^3J = 7.7 Hz, H_m), 5.48 (d, 1H, ^3J = 7.8 Hz, H_l). HRMS (ESI): m/z = 955.9274 [$(M)^+$] (calcd for $C_{42}H_{26}N_5O_6$ $Ru^{80}Se_2^+$: m/z = 955.9281). Anal. Calcd for $C_{42}H_{26}N_6O_9RuSe_2{\cdot}4H_2O$: C, 46.29; H, 3.14; N, 7.71. Found: C, 45.99; H, 2.84; N, 7.56.

Physical Methods. Elemental analysis (EA), electrospray ionization mass spectrometry (ESI-MS), matrix-assisted laser desorption/ionization mass spectrometry (MALDI-TOF), and electron impact (EI) mass spectrometry data were collected at the Chemistry Instrumentation Facility of the University of Calgary. Electrochemical measurements on dyes in solution were performed under anaerobic conditions with a Princeton Applied Research VersaStat 3 potentiostat using dry solvents, a glassy carbon working electrode, a platinum counter electrode, a silver pseudoreference electrode, and a 0.1 M NBu_4BF_4 supporting electrolyte. Electronic spectroscopic data were collected on MeCN solutions using a Cary 5000 UV−vis spectrophotometer (Varian).

Sensitized TiO_2 Substrate Preparation. Mesoporous nanocrystalline TiO_2 thin films were deposited onto microscope glass slides (for spectroscopic study) or fluorine-doped tin oxide (FTO) substrate (for electrochemistry) as previously described.[20] The films were then immersed in methanol solution containing ~1 × 10^{-4} M dye molecules and 1 equiv of tetrabutylammonium hydroxide for ~20 min to achieve a surface coverage of ~2 × 10^{-8} mol/cm^2. The sensitized films were then washed with neat methanol and acetonitrile. The films were diagonally positioned in a standard 1 cm^2 quartz cuvette with electrolyte and purged with argon gas for at least 30 min prior to experimentation.

Spectroelectrochemistry. Steady-state UV−vis absorption spectra were obtained on a Varian Cary 50 spectrophotometer at room temperature. A potentiostat (BAS model CV-50W) was employed for measurements in a standard three-electrode configuration with a sensitized TiO_2/FTO working electrode, a platinum disk counter electrode, and a Ag/AgCl reference electrode (Bioanalytical Scientific Instruments, Inc.) in 0.5 M $LiClO_4/CH_3CN$ solution. All potentials were reported versus the normal hydrogen electrode (NHE). The ferrocenium/ferrocene half-wave potential was measured at room temperature before and after each experiment and was used as an external standard to calibrate the reference electrode. Conversion constant of −640 mV from NHE to Fc^+/Fc was used in acetonitrile at 25 °C.[21]

Transient Absorption Spectroscopy. Nanosecond transient absorption measurements were acquired with an apparatus similar to that which has been previously described.[20] Briefly, samples were excited by a frequency-doubled Q-switched, pulsed Nd:YAG laser (Quantel USA (BigSky) Brilliant B; 532 nm, 5−6 ns full width at half-maximum (fwhm), 1 Hz, ~10 mm in diameter) directed 45° to the film surface. A 150 W xenon arc lamp served as the probe beam (Applied Photophysics) that was aligned orthogonally to the excitation light. Detection was achieved with a monochromator (Spex 1702/04) optically coupled to an R928 photomultiplier tube (Hamamatsu). Typically, 30 laser pulses were averaged at each observation wavelength for full spectra generation. Single wavelength kinetic measurement was acquired by 100−200 laser averages. Kinetic data fitting and spectral modeling was performed in Origin 8, and least-squares error minimization was accomplished using the Levenberg−Marquardt iteration method.

Open Circuit Photovoltage Measurements. Sensitized TiO_2/FTO substrate was sandwiched against a platinized FTO counter electrode with a vinyl film (Warps, 8 mil Vinyl-Pane) spacer. Electrolyte containing 0.5 M LiI and 0.05 M I_2 dissolved in CH_3CN was employed. Steady-state light excitation was achieved with the 514.5 nm line of an Innova Ar^+ laser (Coherent). The laser line was expanded by a Thorlabs BE 10X beam expander. Alteration of the incident light irradiance was achieved by using a combination of neutral density filters (Newport). The cell area illuminated was 2.2 cm^2. Photovoltage was measured with a potentiostat (BASi Epsilon-EC, Bioanalytical). Light-soaking was performed to mitigate any hysteresis from the lowest to the highest irradiance and then back and forth until the open circuit photovoltage stabilized (<5 mV) at each irradiance prior to data acquisition. The light-soaking process typically took two cycles.

Computational Methods. The Gaussian 03 computational package[22] was used to perform ground-state geometry optimization calculations employing Becke's three-parameter hybrid exchange functional and the Lee−Yang−Parr nonlocal correlation functional B3LYP[23−25] and LANL2DZ basis set[26,27] with an effective core potential for Ru, and a 6-31G* basis set was used for Se, S, C, N, O, and H atoms.[28] Time-dependent density functional theory (TDDFT) calculations were also performed using this methodology, and the first 60 singlet excited states were calculated. Calculations by the first-principles method were used to obtain accurate excitation energies and oscillator strengths. We modeled the solvent with

Scheme 1. Synthesis of Ligands L1H−L3H[a]

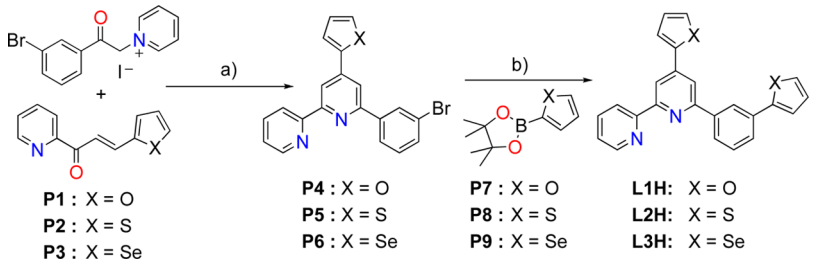

[a]Reaction conditions: (a) ammonium acetate, formamide, 120 °C, 14 h. (b) $Pd(PPh_3)_4$, K_2CO_3, THF/H_2O (9:1), 65 °C, 14 h.

Scheme 2. Synthesis of Metal Complexes Ru−X_{Me} and Ru−X_H[a]

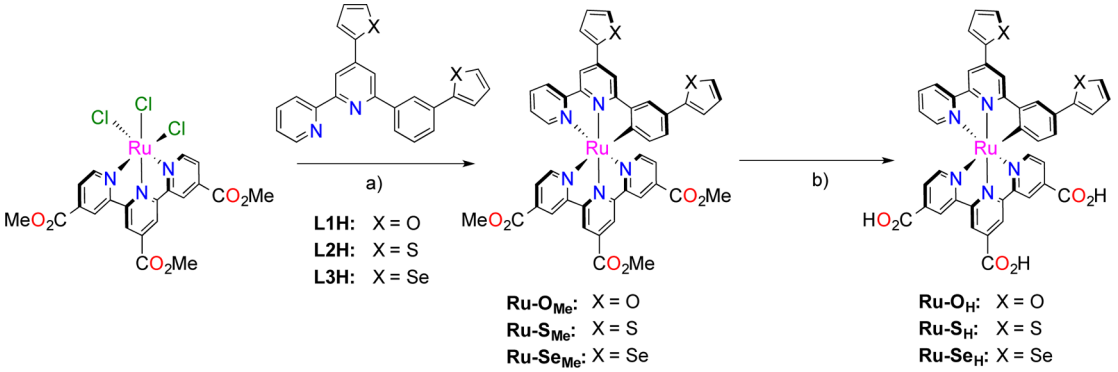

[a]Reaction conditions: (a) MeOH/H_2O/THF (5:1:1 v/v/v), *N*-ethylmorpholine, 65 °C, N_2, 14 h. (b) DMF/NEt_3/H_2O (3:1:1 v/v), reflux, 4 h.

the polarizable continuum model (PCM) using MeCN as the solvent.[29]

RESULTS

Synthesis and Characterization. A modular synthetic approach provided access to the series of tridentate cyclometalating ligands, **L1H−L3H**, on a relatively large scale using established procedures. *Pro*-ligands **P4−P6** were each synthesized upon a Kröhnke condensation of 1-(2-(3-bromophenyl)-2-oxoethyl)pyridinium iodide[16] with **P1−P3**, respectively, to yield the substituted phenyl bipyridine derivatives that were further reacted with Suzuki reagents **P7−P9** to furnish **L1H−L3H** in high yields (Scheme 1). The syntheses of complexes Ru−X_{Me} (X = O, S, Se) followed a previously described protocol[30−33] involving the reaction of Ru(**L4**)Cl_3 with **L1H−L3H**, respectively. The resultant chromatographically pure methyl ester versions of the complexes were acquired in yields ranging from 52 to 78% (Scheme 2). The isomer containing the substituent para to the anionic carbon was isolated in exclusivity in all cases.

The structural identities of all ligands and complexes were confirmed by a combination of NMR spectroscopy, mass spectrometry, or elemental analysis. The ^{1}H NMR spectra for Ru−X_{Me} reveal that the chalcogen heterocycle resonances (H_g, H_h, H_o, H_p) shift progressively downfield for X = O, S, and Se, respectively. The relative electron-donating character is attributed to lesser orbital overlap and elongation of the X—C bonds with the larger chalcogen atoms, resulting in heterocycles possessing more olefinic character.

The Ru^{III}/Ru^{II} reduction potentials for Ru−X_{Me} measured by cyclic voltammetry in MeCN (Table 1) indicate only a slight sensitivity to terminal substituents. The furyl rings appear to act as weakly electron-donating substituents (corroborated by the NMR data); the thiophene and selenophene units have a nominal effect on the Ru(III) reduction potentials. UV−vis absorption spectra recorded on the complexes dissolved in MeCN also reveal a lack of sensitivity to the identity of the chalcogenides (Figure 3). The presence of the five-membered rings benefit light absorption, as evidenced by higher extinction coefficients of the major absorption bands relative to a ruthenium complex not containing the substituents. TD-DFT calculations performed on ground-state optimized structures of the respective dyes indicate four metal-to-ligand charge transfer transitions are responsible for the absorption bands in the visible region (Figure 3).

Table 1. Reduction Potentials of Ru−X (X = O, S, Se) in Solution and on Mesoporous TiO_2

	$E_{1/2}$, Ru(III)/Ru(II) (V vs NHE)	
sample	Ru−X_{Me}[a]	Ru−X/TiO_2[b]
Ru−O	1.014	0.965
Ru−S	1.024	0.950
Ru−Se	1.027	0.954
1[c]	1.028	0.950

[a]Data collected using 0.1 M NBu_4BF_4 MeCN solutions at 100 mV/s and referenced to a $[Fc]/[Fc]^+$ internal standard, followed by conversion to NHE; $[Fc]/[Fc^+]$ = +640 mV vs NHE in MeCN. [b]Data collected using 0.5 M $LiClO_4$ as the electrolyte in MeCN solutions. [c]Benchmark complex: [Ru(pbpy)(**L4**)](NO_3).[31]

Interfacial Charge Recombination in the Absence of Iodide. The respective dyes were immobilized on TiO_2 to interrogate the electron transfer processes at the interface. Nanosecond transient absorption spectroscopy was used to quantify the interfacial electron transfer reactions from $TiO_2(e^-)$ to the oxidized sensitizers (Ru^{III}-X/$TiO_2(e^-)$ →

dx.doi.org/10.1021/jp500879p | J. Phys. Chem. C 2014, 118, 17079−17089

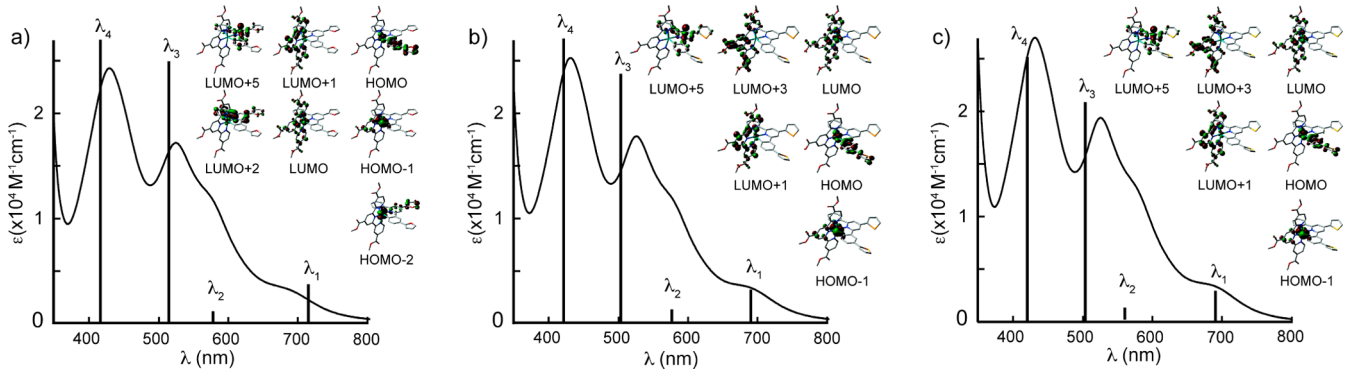

Figure 3. Experimental UV−vis absorption spectrum overlaid with calculated transitions represented by vertical bars (only the transitions with contributions >30% are shown). Details of calculated transitions (theoretical wavelength in nm, oscillator strength, % contribution to transition): (a) Ru−O_{Me}; λ_1, HOMO → LUMO (714, 0.024, 93%); λ_2, HOMO → LUMO+1 (587, 0.009, 64%); λ_3, HOMO-1 → LUMO and HOMO → LUMO +1 (513, 0.172, 51% and 31%); λ_4, HOMO → LUMO+5 and HOMO-2 → LUMO+2 (416, 0.199, 46% and 30%). (b) Ru−S_{Me}; λ_1, HOMO → LUMO (690, 0.026, 94%); λ_2, HOMO → LUMO+1 (575, 0019, 53%); λ_3, HOMO-1 → LUMO and HOMO → LUMO+1 (502, 0.179, 39% and 38%); λ_4, HOMO-1 → LUMO+3 and HOMO → LUMO+5 (420, 0.216, 42% and 41%). (c) Ru−Se_{Me}; λ_1, HOMO → LUMO (691, 0.026, 94%); λ_2, HOMO → LUMO+1 (575, 0.019, 54%); λ_3, HOMO-1 → LUMO and HOMO → LUMO+1 (503, 0.193, 41% and 39%); λ_4, HOMO → LUMO +3 and HOMO → LUMO+5 (421, 0.248, 50% and 40%).

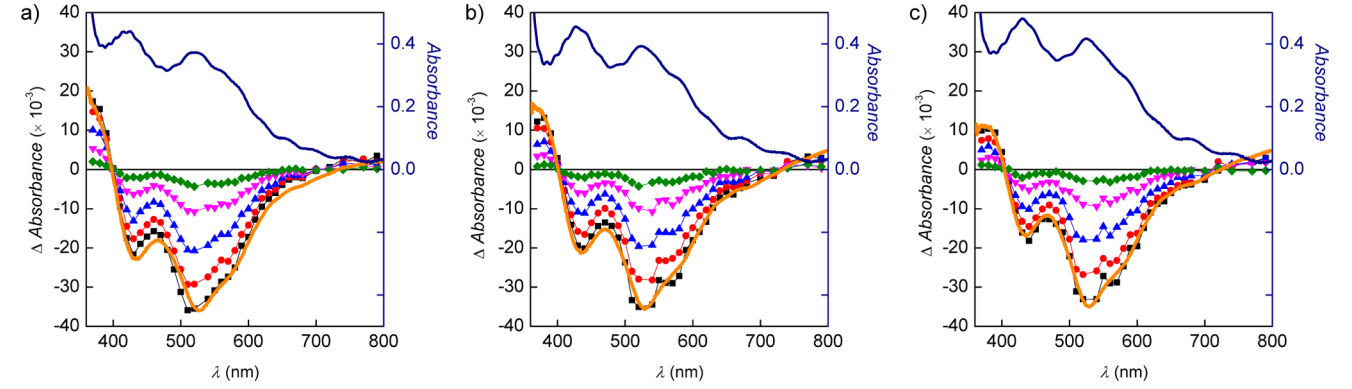

Figure 4. Absorption difference spectra measured at the indicated delay times after pulsed 532 nm excitation (laser fluence, 0.5 mJ/cm^2) of (a) Ru−O/TiO_2 thin film; (b) Ru−S/TiO_2 thin film; and (c) Ru−Se/TiO_2 thin film immersed in 0.5 M $LiClO_4/CH_3CN$. (black squares, 45 ns; red circles, 100 ns; blue triangles, 500 ns; magenta reverse triangles, 5 μs; green diamonds, 50 μs; blue solid traces, ground state absorption spectra with *y*-axis on the right; orange solid curves, simulations based on the difference spectra of Ru^{III}-X/TiO_2 and Ru^{II}-X/TiO_2 by spectroelectrochemistry)

Ru^{II}-X/TiO_2). Absorption difference spectra are shown in Figure 4 for this reaction after pulsed 532 nm laser excitation in 0.5 M $LiClO_4/CH_3CN$.

The immediate appearance of the oxidized dye spectra indicated that the electron injection to TiO_2 acceptor states was ultrafast ($k_{inj} > 10^8$ s^{-1}). Normalizable spectra at all delay times and maintenance of sharp isosbestic points at ∼400 and 720 nm confirmed one charge-separated state: Ru^{III}−$X/TiO_2(e^-)$. Figure 5 shows single wavelength absorption changes that correspond to charge recombination between $TiO_2(e^-)$ and the oxidized sensitizer. A probe wavelength of 583 nm was selected because it allowed for observation of the oxidized sensitizer without complications that arise from the shift of the ground state absorption induced by the injected $TiO_2(e^-)s$[34] (Supporting Information Figure S2). The kinetics were nonexponential but were satisfactorily modeled by Kohlrausch−Williams−Watts (KWW) function,[35,36] eq 1, with a common β value of 0.16. Average rate constants (k_{cr}) were calculated as the first moment by using eq 2. The rate constants were within experimental error the same for all these compounds and, hence, are summarized as one, $k_{cr} = (2.5 \pm 0.6) \times 10^2$ s^{-1}.

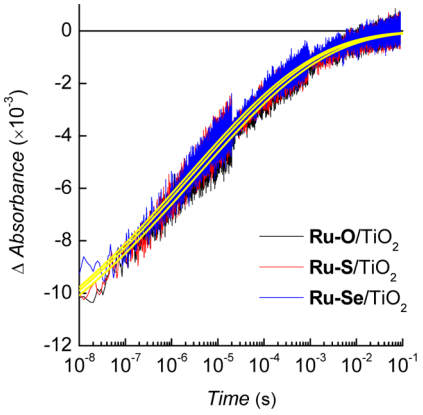

Figure 5. Absorption changes measured after pulsed laser excitation of the sensitized film in 0.5 M $LiClO_4/CH_3CN$. (λ_{exc}, 532 nm; probe, 583 nm; laser fluence, 0.5 mJ/cm^2; ground state absorption at 532 nm, ≈ 0.22). Overlaid in yellow are the best fits to KWW kinetic model.

$$\Delta Abs = A \exp[-(kt)^{\beta}] \quad (1)$$

dx.doi.org/10.1021/jp500879p | J. Phys. Chem. C 2014, 118, 17079−17089

$$k_{cr} = \left[\frac{1}{k\beta} \times \Gamma\left(\frac{1}{\beta}\right)\right]^{-1} \quad (2)$$

Sensitizer Regeneration by Iodide. The regeneration of $Ru^{III}-X/TiO_2(e^-)$ by iodide was investigated with nanosecond transient absorption. A pulsed 532 nm laser was used to generate the interfacial charge separated state, $Ru^{III}-X/TiO_2(e^-)$, in an electrolyte solution containing specific quantities of iodide. The time required for regeneration by iodide was tracked by monitoring the spectral changes at 583 nm (Supporting Information Figure S1), where it represented only recovery of the ground state sensitizer molecules as a function of time. The sensitizer regeneration kinetics have been previous modeled by single-exponential,[37] biexponential[5,38] or KWW[39] functions, but none of them were able to satisfactorily model the data herein. Triexponential function (eq 3) was found to be adequate, and an average observed regeneration rate constant ($\bar{k}_{obs}$) can be obtained by eq 4. The observed regeneration rate constants, $\bar{k}_{obs}$, were linear with respect to iodide concentration (Figure 6), and the linear fitting of the

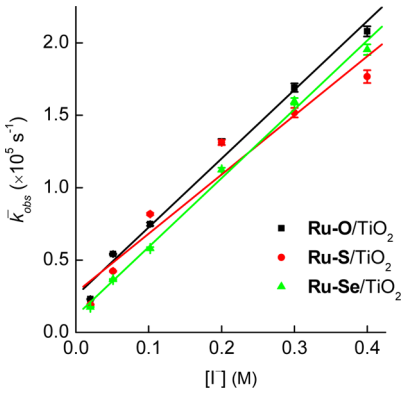

Figure 6. Plot of observed regeneration rate constants ($\bar{k}_{obs}$) of Ru–O/TiO_2 (black squares), Ru–S/TiO_2 (red circles), and Ru–Se/TiO_2 (green triangles) versus titrated iodide (I^-) concentrations.

data indicates that the second-order rate constants (k_{reg}) for dye regeneration are effectively the same (Table 2).

$$\Delta Abs(t) = A_0 + A_1 \exp(-k_1 t) + A_2 \exp(-k_2 t) + A_3 \exp(-k_3 t) \quad (3)$$

$$\bar{k}_{obs} = \frac{A_1/k_1 + A_2/k_2 + A_3/k_3}{A_1/k_1^2 + A_2/k_2^2 + A_3/k_3^2} \quad (4)$$

Table 2. Second-Order Regeneration Rate Constants (k_{reg}) for Ru–X/TiO_2 by I^- in CH_3CN

	Ru–O/TiO_2	Ru–S/TiO_2	Ru–Se/TiO_2
k_{reg} (M^{-1} s^{-1})	$4.7 \pm 0.3 \times 10^5$	$4.1 \pm 0.5 \times 10^5$	$4.7 \pm 0.2 \times 10^5$

Interfacial Charge Recombination in the Presence of Iodide. The open-circuit voltages (V_{oc}) for the sensitized films were measured as a function of incident steady-state monochromatic 514.5 nm light irradiance in the presence of 0.5 M LiI and 0.05 M I_2 in CH_3CN electrolyte (Figure 7). The V_{oc} values showed a linear response with respect to the logarithmic incident light flux described by the diode equation.[40−42] A 59 mV increase of V_{oc} per decade increase

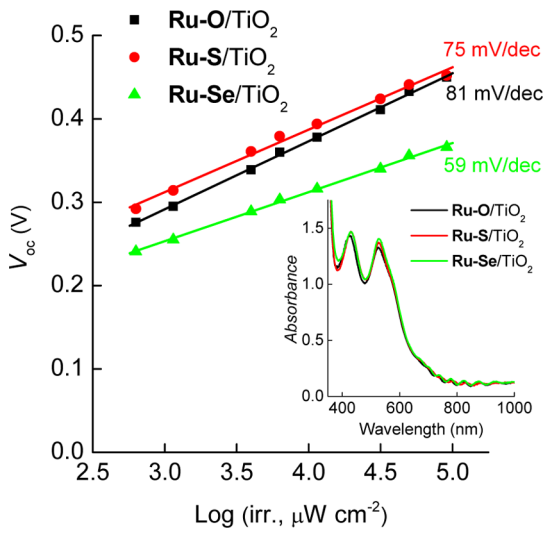

Figure 7. Plot of open circuit voltage as a function of incident steady state monochromatic light (λ_{exc}, 514.5 nm) for Ru–O/TiO_2, Ru–S/TiO_2, and Ru–Se/TiO_2 measured in solar cells containing 0.5 M LiI and 0.05 M I_2 dissolved in CH_3CN. The inset shows the ground state absorption spectra of the three sensitizers anchored on TiO_2/FTO substrate for the measurement.

of the incident light irradiance was also predicted if the ideality factor was 1. Indeed, the solar cell that contained Ru–Se/TiO_2 under our experimental condition showed a V_{oc} response of 59 mV/dec of logarithmic irradiance with reproducibility. Solar cells incorporating Ru–O/TiO_2 or Ru–S/TiO_2 showed slopes of 81 mV/dec or 75 mV/dec, respectively. The slopes corresponded to ideality factors of 1.37 or 1.27.

The strikingly low photovoltages for the selenophenyl derivative prompted us to measure any differences in the acceptor states of TiO_2 for the series of sensitized substrates, but none were found, according to the congruent density of states for the series determined by monitoring the spectral changes of the $TiO_2(e^-)$ as a function of applied potential (Supporting Information Figure S2, S3). The disappearance of photochemically generated I_3^- was monitored by transient absorption at 375 nm (Figure 8), where I_3^- absorbed strongly

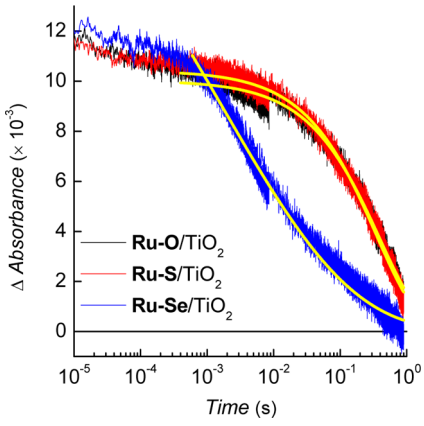

Figure 8. Absorption changes measured after pulsed laser excitation of the sensitized films in 0.4 M LiI + 0.1 M $LiClO_4/CH_3CN$ (λ_{exc}, 532 nm; probe, 375 nm; laser fluence, 2.8 mJ/cm^2; ground state absorptions at 532 nm, ≈0.26). The sensitized films were electrochemically biased to −240 mV vs NHE. Overlaid in yellow are the best fits to the KWW kinetic model.

dx.doi.org/10.1021/jp500879p | J. Phys. Chem. C 2014, 118, 17079−17089

($\varepsilon \sim 19\,000\ M^{-1}\ cm^{-1}$).[43] Triiodide was assumed to be consumed by $TiO_2(e^-)$ by one-electron reduction to form 1 equiv of diiodide ($I_2^{\bullet -}$) and I^-.[14,44] This recombination reaction occurred in the millisecond-to-second time scale with kinetics that were best modeled by the KWW function (eq 1). Note that to increase the recombination rate, excess electrons were introduced into the TiO_2 thin film with a potentiostat. The negative applied potential corresponded to ~20−25 electrons per TiO_2 nanocrystallite on the basis of spectroelectrochemical data shown in Supporting Information Figure S3. The average recombination rate constants ($\overline{k}'_{cr}$) were calculated using eq 2. The rate constants and β' are summarized in Table 3. To ensure that the results were general to many $TiO_2(e^-)$ concentrations, the recombination studies were completed at three different bias conditions (Supporting Information Figure S4).

Table 3. Rate Constants for Charge Recombination between $TiO_2(e^-)$ and I_3^- for Ru−X/TiO_2[a]

	Ru−O/TiO_2	Ru−S/TiO_2	Ru−Se/TiO_2
$\overline{k}'_{cr}$ (s^{-1})	1.94	2.18	10.8
β'	0.68	0.68	0.22

[a]Data were fit to eqs 1 and 2.

DISCUSSION

The most common ruthenium-based dyes in the literature are derivatives of **N3** and therefore contain a chalcogen atom in the donor portion of the molecule.[2,4] It has been asserted that the most likely site of adduct formation with the electrolyte species is at or near the isothiocyanato ligands.[45] This claim resonates with our previous analysis of organic dyes that show faster rates of dye regeneration when sulfur atoms reside within the donor unit instead of oxygen atoms.[5] These collective observations support the notion that the sulfur atoms of **N3** help to mediate dye regeneration by the electrolyte. However, there exists no direct spectroscopic proof for this claim in the literature because the direct measurement of dye−electrolyte interactions, in which the heteroatoms in the donor units of ruthenium dyes are systematically modified, has not yet been demonstrated. A study that modifies the chalcogen of the isothiocyanato ligand is not only a synthetically challenging endeavor, it would also lead to disparate frontier molecular orbital energies that would preclude an accurate evaluation of relative dye generation and charge recombination kinetics.

The three ruthenium dyes investigated in this study sidestep said challenges because each member of the series contains nearly energetically degenerate frontier molecular orbitals, despite differing in the identity of the chalcogen that compromises the donor portion of the molecule. It is over the donor fragment of the molecule that the HOMO resides (as well as the singly occupied molecular orbital of the Ru^{III}−X, which is more relevant to the regeneration step; Supporting Information Figure S5) and thus is the most likely site of adduct formation with the electrolyte. The optical properties for the three complexes are effectively superimposable, and the HOMO energies are almost the same for the series, both in solution and on titania. These features therefore enable the unprecedented opportunity to measure charge-transfer kinetics for a series of ruthenium dyes, with different atoms in the donor unit, where absorptivities and redox parameters are held effectively at parity.

A key structural feature enabling this particular study is the replacement of the isothiocyanato ligands with a cyclometalating ligand. Because the aryl ring of this chelating anionic ligand acts as a strong donor, the HOMO is delocalized over the metal, the aryl ring, and terminal substituents attached to the aryl ring. The Ru(III) reduction potential is typically sensitive to substituents attached to the aryl ring—particularly those para to the carbanion—but the electrochemical properties of Ru−X indicate that the identity of the chalcogen in the five-membered aromatic rings does not significantly affect the electron density at the metal center. (The five-membered ring attached to the less-electron-rich pyridine ring of the chelating ligand compromises the HOMO-2 level and is therefore not expected to influence the metal-based reduction potentials.) Optical profiles were also found to be the same for the Ru—X series, with the bands in the visible region arising from transitions from the metal−aryl−substituent portion of the molecule to the tridentate ligand bearing the anchoring groups. This scenario satisfies a key aspect of sensitization in that the donor unit resides away from the semiconductor surface, a feature that benefits dye regeneration, and the excited-state electron density resides between the surface and the ruthenium center to enable facile electron injection.

Attachment of each of the dyes to anatase mesoporous titania leads to minor but expected changes in optical and electrochemical properties, reflecting the slight differences in electron donating character of the anchoring ligand upon absorption to the surface. The ground state absorption spectra for Ru−X/TiO_2 recorded in MeCN had the same response to lithium cations and were not affected by changes in the concentration of iodide or triiodide within experimental uncertainty (Supporting Information Figures S6−S8). Quantitative electron injection into the sensitized thin films was observed for each member of the series at rates of $>10^8\ s^{-1}$, and the rates of dye regeneration by the $TiO_2(e^-)$ were found to be the same for the series. Spectroelectrochemistry also revealed that the electrochemical reduction of the titania was insensitive to the identity of the surface-anchored dye molecules (Supporting Information Figure S2). These collective features set the stage for studying the interaction of Ru^{III}-X/TiO_2 with the iodide electrolyte without needing to account for differences in light absorption and energy levels of the dye−semiconductor.

There were no observable ground state absorption changes when either iodide or triiodide was titrated into the reaction vessel containing Ru−X/TiO_2 (Supporting Information Figures S7, S8). The generation of the interfacial charge-separated state, Ru^{III}−X/$TiO_2(e^-)$, in an electrolyte solution containing specific quantities of iodide revealed regeneration rate constants, $\overline{k}_{obs}$, that were within experimental error the same (Figure 6 and Table 2); however, the reaction of Ru^{III}−X/$TiO_2(e^-)$ with triiodide to form $I_2^{\bullet -}$ and I^- revealed a clear sensitivity to X. This reaction was found to occur with an average recombination rate constant ($\overline{k}'_{cr}$) of 1.94 s^{-1} for Ru^{III}−O/$TiO_2(e^-)$ and 2.18 s^{-1} for Ru^{III}−S/$TiO_2(e^-)$, but was 10.8 s^{-1} for the reaction of Ru^{III}−Se/$TiO_2(e^-)$ with triiodide. This finding suggests that selenium plays a role in mediating the interaction of I_3^- with the semiconductor surface, a feature that is corroborated by the distinctively lower photovoltages for Ru−Se/TiO_2 relative to the other members of the series.

This collective data indicates that modifying the chalcogen atom in the series of dyes does not impact the regeneration of the oxidized dye by the electrolyte. This finding is not aligned with our examination of organic dyes that showed dye

dx.doi.org/10.1021/jp500879p | J. Phys. Chem. C 2014, 118, 17079−17089

regeneration was sensitive to atoms in the donor unit.[5] We attribute these differences in measurements to the chalcogen hybridization of Ru−X/TiO_2 relative to those in the organic dyes presented in Figure 1. Another factor to consider is that Ru−X/TiO_2 contains a chalcogen atom that is not attached to the aryl ring, thereby offering a second binding site not within the donor fragment of the dye that could preclude resolution of the regeneration step. Future studies will address this issue by excluding substituents attached to the pyridine ring of the chelating ligand.

The data clearly shows that the chalcogen atoms do effect the interaction between the surface and the electrolyte, a finding that resonates with an earlier study by O'Regan and co-workers indicating that the higher affinity for iodine to bind to sp^3-hybridized chalcogen atoms leads to faster recombination rates.[8] Although we had not anticipated that positioning the chalcogens within the donor unit would affect recombination, the molecular structures of Ru−X do allow for the chalcogen to reside close to the semiconductor surface. This proximity could therefore enhance adduct formation close to the semiconductor surface, thereby enabling more facile recombination with $TiO_2(e^-)$ and compromising the photovoltages. This finding calls attention to the need to position atoms capable of interacting with the oxidized iodide species in the electrolyte away from the surfaces.

CONCLUSION

The Ru−X cycloruthenated sensitizers reported here provided a means to interrogate the influence of chalcogen atoms on interfacial electron transfer events that occur following light-induced electron injection into titania. It was spectroscopically determined in titration experiments that the reaction between triiodide and $TiO_2(e^-)$ was ∼5-fold faster in the case of Ru−Se/TiO_2 relative to the dyes containing furyl and thiophene substituents. This feature and the correspondingly lower measured photovoltage is ascribed to the heterocycle fostering adduct formation with oxidized iodide near the semiconductor surface. Differences in reaction rates for dye regeneration were not observed for the series, despite a variance in atom identity in the donor fragment of the molecule. We conjecture that the congruency in dye regeneration rates for the series is due to the basicities of the heterocycles' being too similar or the presence of the heterocycle not attached to the aryl ring precluding resolution of regeneration at the donor unit.

ASSOCIATED CONTENT

Supporting Information

Additional spectroscopic data and DFT calculations of molecular orbitals. This material is available free of charge via the Internet at http://pubs.acs.org.

AUTHOR INFORMATION

Corresponding Authors

*E-mail: rarratia@unab.cl.
*E-mail: gjmeyer@unc.edu
*E-mail: cberling@chem.ubc.ca.

Present Address

G.J.M.: The University of North Carolina at Chapel Hill, Chemistry Department, CB 3290, Chapel Hill, NC 27599-3290.

Notes

The authors declare no competing financial interest.

ACKNOWLEDGMENTS

G.J.M. and K.H. acknowledge support by a grant from the Division of Chemical Sciences, Office of Basic Energy Sciences, Office of Energy Research, U.S. Department of Energy (DE-FG02-96ER14662). K.H. acknowledges a Johns Hopkins University Harry and Cleio Greer Fellowship. The Canadian authors are grateful to Canadian Natural Science and Engineering Research Council, Canadian Foundation for Innovation, Alberta Ingenuity, and the Canada School of Energy and Environment (CSEE) for support. E.S. and R.A. thank FONDECYT 1110758, 1130707, RC120001 de la Iniciativa Científica Milenio del Ministerio de Economía, Fomento y Turismo.

REFERENCES

(1) O'Regan, B.; Grätzel, M. A Low-Cost, High-Efficiency Solar Cell Based on Dye-Sensitized Colloidal TiO_2 Films. *Nature* **1991**, *353*, 737−740.

(2) Ardo, S.; Meyer, G. J. Photodriven Heterogeneous Charge Transfer with Transition-Metal Compounds Anchored to TiO_2 Semiconductor Surfaces. *Chem. Soc. Rev.* **2009**, *38*, 115−164.

(3) Nazeeruddin, M. K.; Kay, A.; Rodicio, I.; Humphry-Baker, R.; Mueller, E.; Liska, P.; Vlachopoulos, N.; Graetzel, M. Conversion of Light to Electricity by cis-X_2bis(2,2′-bipyridyl-4,4′-dicarboxylate)-ruthenium(II) Charge-Transfer Sensitizers (X = Cl^-, Br^-, I^-, CN−, and SCN^-) on Nanocrystalline Titanium Dioxide Electrodes. *J. Am. Chem. Soc.* **1993**, *115*, 6382−6390.

(4) Grätzel, M. Recent Advances in Sensitized Mesoscopic Solar Cells. *Acc. Chem. Res.* **2009**, *42*, 1788−1798.

(5) Robson, K. C. D.; Hu, K.; Meyer, G. J.; Berlinguette, C. P. Atomic Level Resolution of Dye Regeneration in the Dye-Sensitized Solar Cell. *J. Am. Chem. Soc.* **2013**, *135*, 1961−1971.

(6) Li, F.; Jennings, J. R.; Wang, Q. Determination of Sensitizer Regeneration Efficiency in Dye-Sensitized Solar Cells. *ACS Nano* **2013**, *7*, 8233−8242.

(7) McCall, K. L.; Morandeira, A.; Durrant, J.; Yellowlees, L. J.; Robertson, N. Characterisation of a Ruthenium Bipyridyl Dye Showing a Long-Lived Charge-Separated State on TiO_2 in the Presence of I^-/I3. *Dalton Trans.* **2010**, *39*, 4138−4145.

(8) O'Regan, B. C.; Walley, K.; Juozapavicius, M.; Anderson, A.; Matar, F.; Ghaddar, T.; Zakeeruddin, S. M.; Klein, C.; Durrant, J. R. Structure/Function Relationships in Dyes for Solar Energy Conversion: A Two-Atom Change in Dye Structure and the Mechanism for Its Effect on Cell Voltage. *J. Am. Chem. Soc.* **2009**, *131*, 3541−3548.

(9) Richards, C. E.; Anderson, A. Y.; Martiniani, S.; Law, C.; O'Regan, B. C. The Mechanism of Iodine Reduction by TiO_2 Electrons and the Kinetics of Recombination in Dye-Sensitized Solar Cells. *J. Phys. Chem. Lett.* **2012**, *3*, 1980−1984.

(10) Nguyen, W. H.; Bailie, C. D.; Burschka, J.; Moehl, T.; Grätzel, M.; McGehee, M. D.; Sellinger, A. Molecular Engineering of Organic Dyes for Improved Recombination Lifetime in Solid-State Dye-Sensitized Solar Cells. *Chem. Mater.* **2013**, *25*, 1519−1525.

(11) Liu, J.; Zhou, D.; Wang, F.; Fabregat-Santiago, F.; Miralles, S. G.; Jing, X.; Bisquert, J.; Wang, P. Joint Photophysical and Electrical Analyses on the Influence of Conjugation Order in D-π-A Photosensitizers of Mesoscopic Titania Solar Cells. *J. Phys. Chem. C* **2011**, *115*, 14425−14430.

(12) Boschloo, G.; Hagfeldt, A. Characteristics of the Iodide/Triiodide Redox Mediator in Dye-Sensitized Solar Cells. *Acc. Chem. Res.* **2009**, *42*, 1819−1826.

(13) Clifford, J. N.; Palomares, E.; Nazeeruddin, M. K.; Grätzel, M.; Durrant, J. R. Dye Dependent Regeneration Dynamics in Dye Sensitized Nanocrystalline Solar Cells: Evidence for the Formation of a Ruthenium Bipyridyl Cation/Iodide Intermediate. *J. Phys. Chem. C* **2007**, *111*, 6561−6567.

(14) Rowley, J. G.; Farnum, B. H.; Ardo, S.; Meyer, G. J. Iodide Chemistry in Dye-Sensitized Solar Cells: Making and Breaking I−I

Bonds for Solar Energy Conversion. *J. Phys. Chem. Lett.* **2010**, *1*, 3132−3140.
(15) Hong, P. C.; Chen, L. J.; Lai, T. Y.; Yang, H. Y.; Chiang, S. J.; Lu, Y. Y.; Tsai, P. K.; Hsu, H. Y.; Wei, W. Y.; Liao, C. B. Synthesis of Selenophene Derivatives as Novel CHK1 Inhibitors. *Bioorg. Med. Chem. Lett.* **2010**, *20*, 5065−5068.
(16) Sasaki, I.; Vendier, L.; Sournia-Saquet, A.; Lacroix, P. G. Facile Synthesis of Cyclometalated Ruthenium Complexes with Substituted Phenylpyridines. *Eur. J. Inorg. Chem.* **2006**, 3294−3302.
(17) Zhao, L. X.; Kim, T. S.; Ahn, S. H.; Kim, T. H.; Kim, E. K.; Cho, W. J.; Choi, H.; Lee, C. S.; Kim, J. A.; Jeong, T. C.; et al. Synthesis, Topoisomerase I Inhibition and Antitumor Cytotoxicity of 2,2′:6′,2″-, 2,2′:6′,3″- and 2,2:6′,4″-terpyridine Derivatives. *Bioorg. Med. Chem. Lett.* **2001**, *11*, 2659−2662.
(18) Ebner, D. C.; Bagdanoff, J. T.; Ferreira, E. M.; McFadden, R. M.; Caspi, D. D.; Trend, R. M.; Stoltz, B. M. The Palladium-Catalyzed Aerobic Kinetic Resolution of Secondary Alcohols: Reaction Development, Scope, and Applications. *Chem.—Eur. J.* **2009**, *15*, 12978−12992.
(19) Dienes, Y.; Durben, S.; Karpati, T.; Neumann, T.; Englert, U.; Nyulaszi, L.; Baumgartner, T. Selective Tuning of the Band Gap of Pi-Conjugated dithieno[3,2-b:2′,3′-d]phospholes Toward Different Emission Colors. *Chem.—Eur. J.* **2007**, *13*, 7487−7500.
(20) Argazzi, R.; Bignozzi, C. A.; Heimer, T. A.; Castellano, F. N.; Meyer, G. J. Enhanced Spectral Sensitivity from Ruthenium(II) Polypyridyl Based Photovoltaic Devices. *Inorg. Chem.* **1994**, *33*, 5741−5749.
(21) Pavlishchuk, V. V.; Addison, A. W. Conversion Constants for Redox Potentials Measured Versus Different Reference Electrodes in Acetonitrile Solutions at 25°C. *Inorg. Chim. Acta* **2000**, *298*, 97−102.
(22) Frisch, M. J.; Trucks, G. W.; Schlegel, H. B.; Scuseria, G. E.; Robb, M. A.; Cheeseman, J. R.; Montgomery, J. A.; Vreven, T.; Kudin, K. N.; Burant, J. C.; Millam, J. M.; Iyengar, S. S.; Tomasi, J.; Barone, V.; Mennucci, B.; Cossi, M.; Scalmani, G.; Rega, N.; Petersson, G. A.; Nakatsuji, H.; Hada, M.; Ehara, M.; Toyota, K.; Fukuda, R.; Hasegawa, J.; Ishida, M.; Nakajima, T.; Honda, Y.; Kitao, O.; Nakai, H.; Klene, M.; Li, X.; Knox, J. E.; Hratchian, H. P.; Cross, J. B.; Bakken, V.; Adamo, C.; Jaramillo, J.; Gomperts, R.; Stratmann, R. E.; Yazyev, O.; Austin, A. J.; Cammi, R.; Pomelli, C.; Ochterski, J. W.; Ayala, P. Y.; Morokuma, K.; Voth, G. A.; Salvador, P.; Dannenberg, J. J.; Zakrzewski, V. G.; Dapprich, S.; Daniels, A. D.; Strain, M. C.; Farkas, O.; Malick, D. K.; Rabuck, A. D.; Raghavachari, K.; Foresman, J. B.; Ortiz, J. V.; Cui, Q.; Baboul, A. G.; Clifford, S.; Cioslowski, J.; Stefanov, B. B.; Liu, G.; Liashenko, A.; Piskorz, P.; Komaromi, I.; Martin, R. L.; Fox, D. J.; Keith, T.; Laham, A.; Peng, C. Y.; Nanayakkara, A.; Challacombe, M.; Gill, P. M. W.; Johnson, B.; Chen, W.; Wong, M. W.; Gonzalez, C.; Pople, J. A., *Gaussian 03, Revision C.02*; Gaussian Inc.: Wallingford, CT, 2004.
(23) Becke, A. D. A New Mixing of Hartree-Fock and Local Density-Functional Theories. *J. Chem. Phys.* **1993**, *98*, 1372−1377.
(24) Becke, A. D. Density-Functional Exchange-Energy Approximation with Correct Asymptotic-Behavior. *Phys. Rev. A* **1988**, *38*, 3098−3100.
(25) Lee, C. T.; Yang, W. T.; Parr, R. G. Development of the Colle-Salvetti Correlation-Energy Formula into a Functional of the Electron-Density. *Phys. Rev. B* **1988**, *37*, 785−789.
(26) Hay, P. J.; Wadt, W. R. Ab Initio Effective Core Potentials for Molecular Calculations − Potentials for the Transition-Metal Atoms Sc to Hg. *J. Chem. Phys.* **1985**, *82*, 270−283.
(27) Wadt, W. R.; Hay, P. J. Abinitio Effective Core Potentials for Molecular Calculations − Potentials for Main Group Elements Na to Bi. *J. Chem. Phys.* **1985**, *82*, 284−298.
(28) Rassolov, V. A.; Ratner, M. A.; Pople, J. A.; Redfern, P. C.; Curtiss, L. A. 6-31G*Basis Set for Third-Row Atoms. *J. Comput. Chem.* **2001**, *22*, 976−984.
(29) Cossi, M.; Scalmani, G.; Rega, N.; Barone, V. New Developments in the Polarizable Continuum Model for Quantum Mechanical and Classical Calculations on Molecules in Solution. *J. Chem. Phys.* **2002**, *117*, 43−54.
(30) Constable, E. C.; Hannon, M. J. Solvent Effects in the Reactions of 6-Phenyl-2,2′-Bipyridine with Ruthenium(II). *Inorg. Chim. Acta* **1993**, *211*, 101−110.
(31) Koivisto, B. D.; Robson, K. C. D.; Berlinguette, C. P. Systematic Manipulation of the Light-Harvesting Properties for Tridentate Cyclometalated Ruthenium(II) Complexes. *Inorg. Chem.* **2009**, *48*, 9644−9652.
(32) Robson, K. C. D.; Koivisto, B. D.; Yella, A.; Sporinova, B.; Nazeeruddin, M. K.; Baumgartner, T.; Grätzel, M.; Berlinguette, C. P. Design and Development of Functionalized Cyclometalated Ruthenium Chromophores for Light-Harvesting Applications. *Inorg. Chem.* **2011**, *50*, 5494−5508.
(33) Robson, K. C. D.; Sporinova, B.; Koivisto, B. D.; Schott, E.; Brown, D. G.; Berlinguette, C. P. Systematic Modulation of a Bichromic Cyclometalated Ruthenium(II) Scaffold Bearing a Redox-Active Triphenylamine Constituent. *Inorg. Chem.* **2011**, *50*, 6019−6028.
(34) Ardo, S.; Sun, Y.; Staniszewski, A.; Castellano, F. N.; Meyer, G. J. Stark Effects After Excited-State Interfacial Electron Transfer at Sensitized TiO_2 Nanocrystallites. *J. Am. Chem. Soc.* **2010**, *132*, 6696−6709.
(35) Williams, G.; Watts, D. C. Non-Symmetrical Dielectric Relaxation Behaviour Arising from a Simple Empirical Decay Function. *Trans. Faraday Soc.* **1970**, *66*, 80−85.
(36) Lindsey, C. P.; Patterson, G. D. Detailed Comparison of the Williams−Watts and Cole−Davidson Functions. *J. Chem. Phys.* **1980**, *73*, 3348−3357.
(37) Nusbaumer, H.; Moser, J.-E.; Zakeeruddin, S. M.; Nazeeruddin, M. K.; Grätzel, M. CoII(dbbip)22+ Complex Rivals Tri-iodide/Iodide Redox Mediator in Dye-Sensitized Photovoltaic Cells. *J. Phys. Chem. B* **2001**, *105*, 10461−10464.
(38) Martiniani, S.; Anderson, A. Y.; Law, C.; O'Regan, B. C.; Barolo, C. New Insight Into the Regeneration Kinetics of Organic Dye Sensitised Solar Cells. *Chem. Commun.* **2012**, *48*, 2406−2408.
(39) Anderson, A. Y.; Barnes, P. R. F.; Durrant, J. R.; O'Regan, B. C. Quantifying Regeneration in Dye-Sensitized Solar Cells. *J. Phys. Chem. C* **2011**, *115*, 2439−2447.
(40) Kumar, A.; Santangelo, P. G.; Lewis, N. S. Electrolysis of Water at Strontium Titanate ($SrTiO_3$) Photoelectrodes: Distinguishing Between the Statistical and Stochastic Formalisms for Electron-Transfer Processes in Fuel-Forming Photoelectrochemical Systems. *J. Phys. Chem.* **1992**, *96*, 834−842.
(41) Huang, S. Y.; Schlichthörl, G.; Nozik, A. J.; Grätzel, M.; Frank, A. J. Charge Recombination in Dye-Sensitized Nanocrystalline TiO_2 Solar Cells. *J. Phys. Chem. B* **1997**, *101*, 2576−2582.
(42) Clark, C. C.; Meyer, G. J.; Wei, Q.; Galoppini, E. Tuning Open Circuit Photovoltages with Tripodal Sensitizers. *J. Phys. Chem. B* **2006**, *110*, 11044−11046.
(43) Gardner, J. M.; Abrahamsson, M.; Farnum, B. H.; Meyer, G. J. Visible Light Generation of Iodine Atoms and I−I Bonds: Sensitized I^- Oxidation and I_3^- Photodissociation. *J. Am. Chem. Soc.* **2009**, *131*, 16206−16214.
(44) Rowley, J. G.; Meyer, G. J. Di- and Tri-Iodide Reactivity at Illuminated Titanium Dioxide Interfaces. *J. Phys. Chem. C* **2011**, *115*, 6156−6161.
(45) Privalov, T.; Boschloo, G.; Hagfeldt, A.; Svensson, P. H.; Kloo, L. A Study of the Interactions Between I(−)/I(3)(−) Redox Mediators and Organometallic Sensitizing Dyes in Solar Cells. *J. Phys. Chem. C* **2009**, *113*, 783−790.